

Deposition of polyaniline films by microwave-assisted chemical bath deposition: effect of acid and monomer concentration

Marcos Fabio Farias Souza¹; Liliane Oliveira Mota²; Iara de Fátima Gimenez³

¹Department of Chemical Engineering, Federal University of Sergipe, São Cristóvão, 49100-000, Brazil, ORCID: 0000-0001-7618-6751

²Materials Science and Engineering Graduate Program (P2CEM), Federal University of Sergipe, 49100-000, São Cristóvão, Brazil, ORCID: 0000-0001-7722-2953

³Department of Chemistry, Federal University of Sergipe, 49100-000, São Cristóvão, Brazil, ORCID: 0000-0001-7722-2953

ABSTRACT: Supercapacitors are noticeable intermediate technologies between capacitors and second-generation batteries due to the large cyclic stability, power densities higher than batteries and energy densities higher than regular capacitors. Among potential electrode materials for supercapacitors, conducting polymers including polyaniline are attracting attention. Here we applied a central composite circumscribed design to study the effect of the oxidant/monomer ratio and of the acid dopant concentration on the capacitive behavior of polyaniline film electrodes prepared by microwave-assisted chemical bath deposition. The formation of polyaniline emeraldine salt was evidenced by Fourier-transform infrared spectroscopy, while the presence of redox peaks in cyclic voltammetry curves indicated that the mechanism of energy storage has pseudocapacitive character. Surface response plots showed a curved region with maximum specific capacitance value (426.8 F g^{-1}). The combination of the factors leading to the maximum point is known as optimum point and here the coded values corresponding to this point correspond to oxidant/monomer ratio of 1.15 and 1.64 mol L^{-1} concentration of H_2SO_4 .

KEYWORDS supercapacitor, polyaniline, chemical bath deposition, experimental design, response surface.

Date of Submission: 01-01-2023

Date of acceptance: 11-01-2023

I. INTRODUCTION

Challenges related to energy demands and the climate consequences of the use of fossil fuels are requiring urgent actions from countries worldwide toward the search for renewable energy sources and storage technologies. Emerging clean and renewable energy technologies include solar and eolic sources, but the intermittent nature of both makes storage devices necessary for the periods when those sources are off (He e Zhang, 2022). Supercapacitors are noticeable intermediate technologies between regular capacitors and second-generation batteries due to the large cyclic stability, power densities higher than batteries and energy densities higher than regular capacitors.

The performance of supercapacitors depends on the properties of their main components, which include the electrolyte, the separator, the electrode material and the current collector (Yavuz, Yilmaz Erdogan e Zengin, 2020). Electrode materials have been the focus of studies aiming at improving the supercapacitor performance, through optimization of properties including surface area and porosity. Those are key properties that are able to improve the access to electroactive sites as well as the internal transport of electrolyte ions, which would ideally occur across the whole volume of the electrode. Carbon materials, transition metal oxides and conducting polymers are the most attractive classes of materials for use in supercapacitor electrodes (Forouzandeh, Kumaravel e Pillai, 2020). In this context, conducting polymers are considered the most promising among those classes due to high energy densities that result from additional charges supplied by reversible redox reactions (Han e Dai, 2019; Qiu *et al.*, 2020).

Polyaniline (PANI) is considered the most promising conducting polymers due to the high conductivity, low cost, ease of preparation and good stability under ambient conditions (Dinari, Momeni e Goudarzirad, 2016). PANI can be prepared both by oxidative polymerization using oxidating agents and by

electrochemical polymerization in different final shapes (powder, hydrogel and films) and with distinct structures (Han e Dai, 2019). A common preparation approach of commercial electrodes is to coat substrates through the drop casting thermal evaporation method, in which the active material in the powdered form is mixed with the conductive additive and a polymeric binder. However, this mixture usually has a negative impact on the performance of the electrochemical device (Sardana *et al.*, 2022). Thus, several preparation methods are investigated in order to deposit the electrodes without the need of binder, including methods such as chemical bath deposition (CBD). CBD is becoming attractive as a deposition technique due to its simplicity and low processing cost when compared to more sophisticated techniques that demand the use of vacuum or complex apparatus such as electrodeposition (Sengupta, Aggarwal e Raula, 2022; Turan, Zeybekoğlu e Kul, 2019).

Studies regarding PANI deposition onto conductive substrates by CBD were reported (Deshmukh *et al.*, 2011, 2013). This preparation consists in the oxidative polymerization of aniline under acidic conditions in the presence of the substrate immersed into the reaction medium and is usually described by a two-step mechanism: a slow induction period followed by the growth of the polymer chains. Aniline-derived radical cations and their insoluble cyclic dimers are formed and bind together to yield phenazine-based oligomers in the induction period. The immersed substrate adsorbs those oligomers and provides nucleation sites to induce propagation of the polymer chains. Thus, the surface of the substrate is coated by a thin layer of PANI that is progressively exposed to the reaction medium in each deposition cycle, in order for the polymerization to go on and the polymer film to grow thicker (Deshmukh *et al.*, 2015; Sapurina e Stejskal, 2008).

The main deposition parameters are generally the concentration of precursors (monomer, oxidant and dopant), pH, type of substrate, bath temperature, deposition time, among other secondary variables. Changes in those parameters may have a decisive effect on the molecular and supramolecular structures of the films and, consequently, on the electrochemical properties of the electrodes. (Deng *et al.*, 2014; Firda *et al.*, 2021; Qiu *et al.*, 2017, 2020). However, few works apply experimental design tools to investigate the effects of deposition parameters on the electrochemical properties of the electrode films. Thus, here we aim to apply a central composite circumscribed design (CCC) to study the effect of the oxidant/monomer ratio (rOM) and of the acid dopant concentration (Ac) on the capacitive behavior of PANI film electrodes prepared by microwave-assisted CBD.

II. EXPERIMENTAL

A. Materials

Analytical grade ammonium persulfate (APS, Sigma-Aldrich) and sulfuric acid (H₂SO₄, Vetec) were used in PANI preparation. Aniline (ANI, Acros Organics) was distilled under reduced pressure prior to use. All aqueous solutions were prepared with Milli-Q ultrapure water. Stainless steel 304 was sanded with sandpaper, decapped in acid medium, and washed ultrasonically with distilled water for 5 minutes before deposition cycles.

B. Preparation of polyaniline film electrode

PANI film preparation was based on the report by Deshmukh *et al.* (2013), involving chemical oxidation of aniline by ammonium persulfate through microwave-assisted CBD. A jacketed beaker as well as a thermostatic bath were used in order to absorb the excess heat during microwave heating. Rotating reaction system and lower concentration were used in comparison to the literature. Fig. 1 shows an illustrative scheme of the complete preparation of PANI film electrodes. 0.25 mol L⁻¹ APS and 0.15-0.85 mol L⁻¹ ANI solutions were initially prepared in the presence of H₂SO₄ according to the experimental design shown in Tab. 1. Then the previously treated stainless steel substrates (1) were immersed vertically into 7 mL of the precursor solution (in 1:1 proportion of synthesis solutions) in a test tube (2). The tube was placed in the jacketed beaker (3), which was placed over a non-rotating support. The power used in the microwave oven (5) was 70 W, with 10 minutes heating time and mean temperature of the precursor solution was 55 °C. At the end of deposition, the PANI film electrode was washed with distilled water followed by drying, weighing and immersed again in the precursor solution for a new deposition cycle. The whole process is repeated until the final mass of the deposited film reaches 0.39 mg/cm². The remaining reaction mixture after deposition was filtered to removal of solid PANI residues which was washed with distilled water, dried in an oven at 70 °C and stored for characterization.

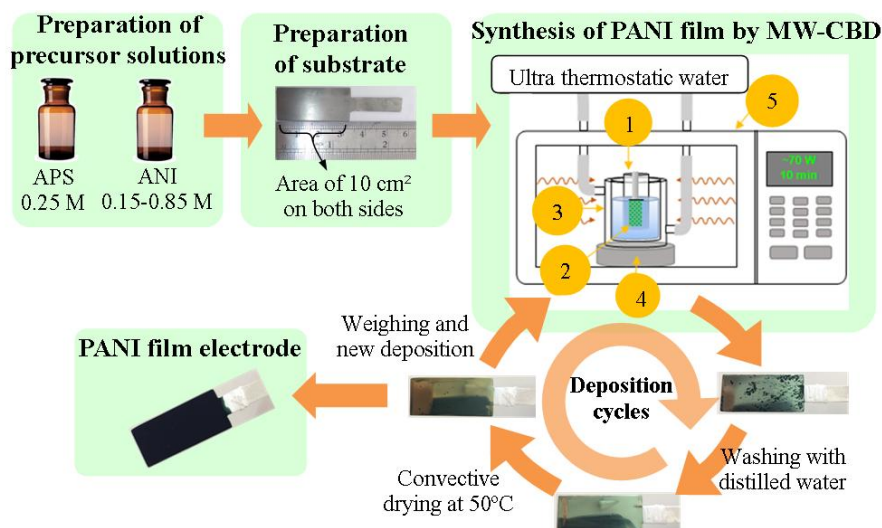


Fig. 1. Illustrative scheme showing the preparation steps used in the deposition of PANI films onto stainless steel electrodes through microwave-assisted chemical bath deposition (MW-CBD).

C. Experimental design

Surface response methodology was used to evaluate the effect of oxidant/monomer molar ratio (rOM) and of the acid dopant concentration (H₂SO₄, Ac) on the specific capacitance of PANI film electrodes. This has been carried out through central composite circumscribed design (CCC) according to conditions summarized in Tab. 2.

Tab. 1. Experimental region containing the factors and their original and coded levels used in the central composite circumscribed design - CCC.

Factors	Code and Actual levels of factors				
	-α	Low	Central	High	+α
	-1.414	-1	0	1	1.414
Oxidant/monomer molar ratio (rOM)	0.29	0.50	1.00	1.50	1.71
Acid dopant, molL ⁻¹ (Ac)	0.19	0.50	1.25	2.00	2.31

Surface response and contour plots were used to evaluate qualitatively the effect of factors on the specific capacitance of PANI films. The empirical model relating the response variable to the factors has been obtained by multiple linear regression (MLR) while the significance of the effects was determined by the analysis of variance (ANOVA). The experimental design and its analysis were carried out using the open software RStudio (version 1.3.1056), which is very useful for data analysis in experimental designs.

Tab. 2. Central composite circumscribed design (CCC) used to evaluate the effect of oxidant/monomer molar ratio (rOM) and of the acid dopant concentration (H₂SO₄, Ac) on the specific capacitance of PANI film electrodes.

Experiment Number	Condition	rOM (-)	Ac (mol L ⁻¹)	ANI (mol L ⁻¹)
1	C1	0.5 (-1)	0.5 (-1)	0.50
2	C2	1.5 (+1)	0.5 (-1)	0.17
3	C3	0.5 (-1)	2.0 (+1)	0.50
4	C4	1.5 (+1)	2.0 (+1)	0.17
5	C0	1.0 (0)	1.25 (0)	0.25
6	C0	1.0 (0)	1.25 (0)	0.25
7	C0	1.0 (0)	1.25 (0)	0.25
8	C5	0.29 (-α)	1.25 (0)	0.85

9	C6	1.71 (α)	1.25 (0)	0.15
10	C7	1.0 (0)	0.19 ($-\alpha$)	0.25
11	C8	1.0 (0)	2.31 (α)	0.25

D. Characterization of materials

Samples were characterized by Fourier transform infrared spectroscopy (FTIR) and cyclic voltammetry (CV) in order to confirm the formation of PANI. FTIR spectra of KBr pellets in the 4000-400 cm^{-1} range were measured using a ShimadzuIRTracer-100 with 8 cm^{-1} resolution and 64 scans. CV curves were measured in order to investigate the capacitive behavior as well as the nature of electrochemical reactions, employing a three-electrode cell configuration containing 1 mol L^{-1} H_2SO_4 solution in aMetrohm Autolab PGSTAT 100N potentiostat/galvanostat operated with the NOVA 2.1.3 software. Saturated calomel electrode (SCE) and a platinum electrode were used as reference and auxiliary electrodes, respectively. Moreover, CV data were used to determine the specific capacitance of the PANI film electrodes, which was chosen as the response variable in the experimental design and was calculated with equation (1) (Venkatesh e Vishista, 2018):

$$C_s = \frac{\int_{E_1}^{E_2} I(E) dE}{2\Delta E \cdot \nu \cdot m} \quad (1)$$

where C_s is the specific capacitance (F g^{-1}); $I(E)$ is the instant current (A); $\Delta E = (E_2 - E_1)$ is the amplitude of the potential range; m is the mass of deposited PANI (g); $\int_{E_1}^{E_2} I(E) dE$ is the integral of the CV curve.

III. RESULTS AND DISCUSSION

A. Preparation of PANI film electrode

PANI film electrodes with final deposited masses around $0.39 \pm 0.02 \text{ mg cm}^{-2}$ were obtained after successive deposition cycles. The change in the mass of films as function of the number of cycles is presented in Fig. 2a and shows that the mass increases linearly with the number of cycles. The deposition rate per cycle for each experimental condition can be estimated from the slope of the deposition curves and can be observed in Fig. 2b, where C8, C5 and C3 conditions led to the highest deposition rates with values of 0.169, 0.145 e 0.135 mg cm^{-2} respectively. For C3 and C8 the behavior is related mainly to the acidity of the reaction medium, as can be observed from a comparison between other groups of conditions, namely C1 and C3 or C7, C0 and C8. During aniline polymerization under strong acidic medium, aniline molecules and its derived radicals are present predominantly in the ionic forms favoring a fast formation kinetics of highly concentrated phenazine oligomers. Those species act as nucleation centers for the subsequent growth of polymer chains (Golba *et al.*, 2020; Peng *et al.*, 2009; Qiu *et al.*, 2017). Thus, a pronounced adsorption of these intermediate species onto the substrate will cause an increased deposition rate of PANI films. On the other hand, the high deposition rate observed for C5 can be mainly related to a lower O/M ratio (i.e. higher aniline concentration) as evidenced upon a comparison between C5, C0 and C6. The kinetics of aniline oxidation has a first order dependence on the monomer concentration in both polymerization steps (Sapurina e Shishov, 2012). In this context, Mello and Mulato (2018) reported that the induction period is reduced as the aniline concentration increases, which results in a higher electrodeposition rate. This behavior can be attributed to a higher availability of aniline molecules to conversion into radical cations which in turn generate nucleation centers and provide higher deposition rates on the substrate surface.

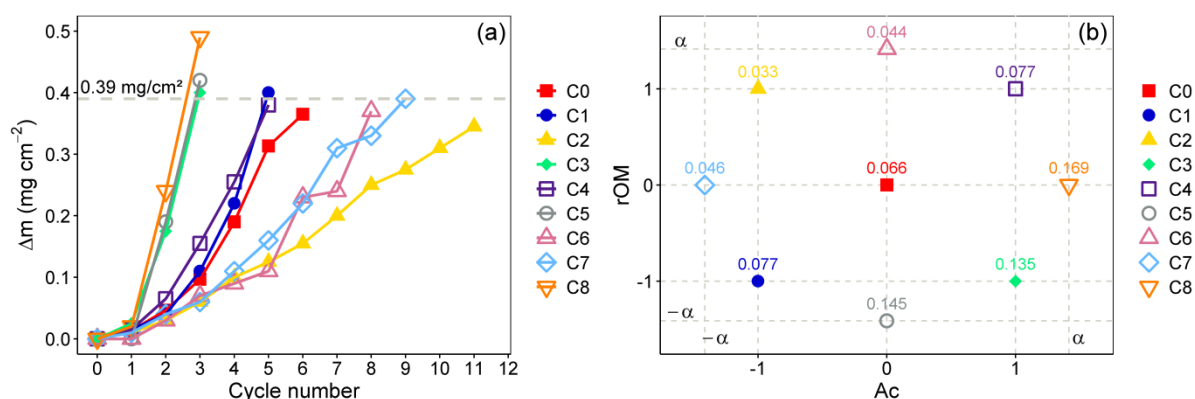


Fig. 2. (a) Change in the mass of PANI films as function of the number of cycles e (b) deposition rate per cycle for all experimental conditions.

B. Characterization of materials

FTIR measurements were carried out to investigate the effect of oxidant/monomer ratio on the molecular structure of PANI prepared under different experimental conditions. Spectra (Fig. 3a) in the $1700\text{-}700 \text{ cm}^{-1}$ show bands that can be assigned to PANI and the respective assignments are in Tab.3. The formation of PANI as emeraldine salt was evidenced by the presence of bands at 1560 cm^{-1} and 1477 cm^{-1} , assigned to C=C stretching from quinoid (Q) and benzenoid (B) rings respectively. The relative intensities of the two bands (I_Q/I_B) is related to the relative proportion of these structures in the polymer chains, thus providing an estimate of the oxidation degree of PANI (Mazzeu *et al.*, 2018; Qiu *et al.*, 2020). I_Q/I_B values in the 0.87-0.99 range for PANI obtained from different reaction conditions can be seen in Fig. 3b where values close to unity characterize a half oxidation state typical of PANI in emeraldine form. It can also be seen that I_Q/I_B values decrease with the increase in acidity, which is particularly evident upon comparison of C7, C0 and C8 conditions in Fig.3b. On the other hand, the increment in oxidant/monomer ratio increases the oxidation degree of PANI which is particularly clear for C5, C0 and C6 conditions in Fig.3b owing to larger relative oxidant amounts. This is in agreement to the trend reported by Abdiryim, Xiao-Gang e Jamal (2005), which showed that both high acid and oxidant concentrations favor high oxidation degrees. Moreover, recent works have confirmed the effect of increasing acidity on the I_Q/I_B value (Golba *et al.*, 2020; Qiu *et al.*, 2020). Additional bands also confirm the presence of emeraldine salt including C-N stretching from secondary aromatic amines ($\sim 1294 \text{ cm}^{-1}$), C-N⁺ stretching from polaronic segments typical of protonated PANI ($\sim 1238 \text{ cm}^{-1}$), in-plane C-H bending from Q=NH⁺-B or B-NH⁺-B groups ($\sim 1120 \text{ cm}^{-1}$); out-of-plane C-H bending from 1,4-disubstituted benzene rings ($\sim 800 \text{ cm}^{-1}$) typical of *para* coupling between units in PANI chains.

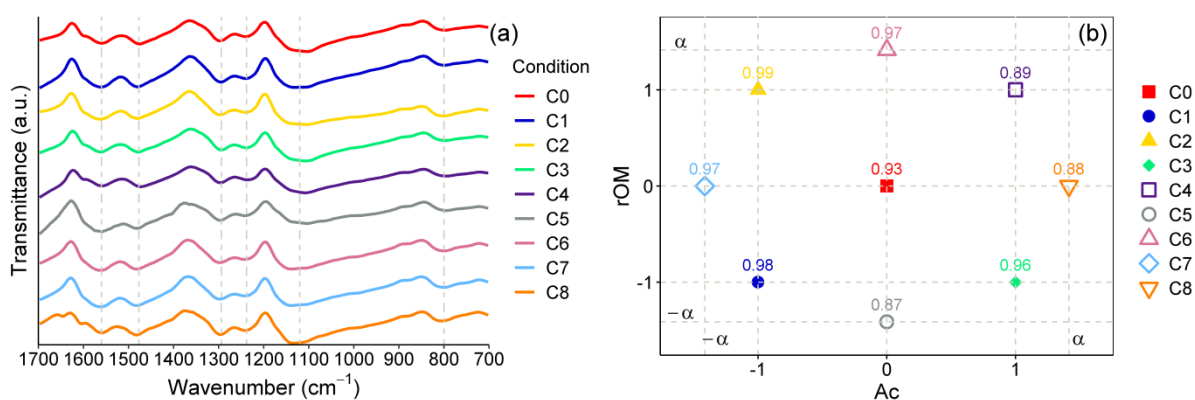


Fig. 3. (a) FTIR spectra e (b) values of I_Q/I_B relative intensities represented as function of the experimental parameters evaluated.

Tab. 3. Position and assignment of FTIR bands shown in Fig.3a.

Wavenumber (cm ⁻¹)	Peak assignment	Reference
1558-1562	C=C stretching in quinoid rings	(Golba <i>et al.</i> , 2020; Qiu <i>et al.</i> , 2020)
1473-1481	C=C stretching in benzenoid rings	(Golba <i>et al.</i> , 2020; Qiu <i>et al.</i> , 2020)
1292-1296	C-N stretching in aromatic secondary amines	(Golba <i>et al.</i> , 2020)
1234-1242	C-N stretching in polaronic segments	(Golba <i>et al.</i> , 2020)
1103-1138	In plane C-H bending from B-N ⁺ -H=Q groups	(Golba <i>et al.</i> , 2020)
794-806	Out-of-plane C-H bending in 1,4 disubstituted benzenic rings	(Golba <i>et al.</i> , 2020; Trchová e Stejskal, 2011)

Electrochemical characterization of PANI film electrodes was carried out by cyclic voltammetry (CV) at the -0.2 to 0.8 V range with potential scan rate of 5 mV s⁻¹ (Fig. 4a). Curves show two pair of redox peaks identified as A/A' and B/B' characteristic of faradaic processes in the films. The position of oxidation peak A varied between 0.24 and 0.29 V for different samples, while A' reduction peaks occurred between 0.06 and 0.12 V (vs. SCE) corresponding to reversible transitions between leucoemeraldine and emeraldine (Santino *et al.*, 2016). The B and B' peaks are present around 0.80 V and 0.63-0.71 V respectively, being related to transitions between the emeraldine and pernigraniline forms (Arulmani, Wu e Anandan, 2019). Peaks appear broadened and less intense for samples prepared under C2 and C7 conditions, reflecting weaker faradaic currents as a result of higher resistance to charge transfer in these films. Redox peaks between 0.5 and 0.55 V related to PANI degradation products including benzoquinone and hydroquinone (Santino *et al.*, 2016) are also present in curves showed in Fig. 4a.

The nature of electrochemical reactions as well as the charge storage capacity of PANI films were evaluated by CV measurements with varying scan rates, particularly using sample C0 (central condition) with values in the 5-100 mV s⁻¹ range (Fig. 4b). Those data are also used as reference of the behavior that is common to all forms and preparation conditions used here. The presence of redox peaks in CV curves indicated that the mechanism of energy storage has pseudocapacitive character (Misnon e Jose, 2017). Shifts of oxidation peak to more positive values and shifts of reduction peaks to more negative values are observed as results of increasing potential scan rate, respectively, being attributed to pseudocapacitive behavior of PANI and its increasing polarization. Moreover, those peaks have their intensities decreased or completely disappear with the increase in scan rate. This is due to the displacement of redox potential to values outside the potential window observed as well as by limitation of electrolyte ion diffusion to reach the electrode surface (Arulmani, Wu e Anandan, 2019; Qiu *et al.*, 2020). Those observations are in agreement with the decreasing trend in the specific capacitance of electrodes (Fig. 4c), suggesting that the system is approaching the full use of electrode material when the specific capacitance is obtained under lowest scan rates.

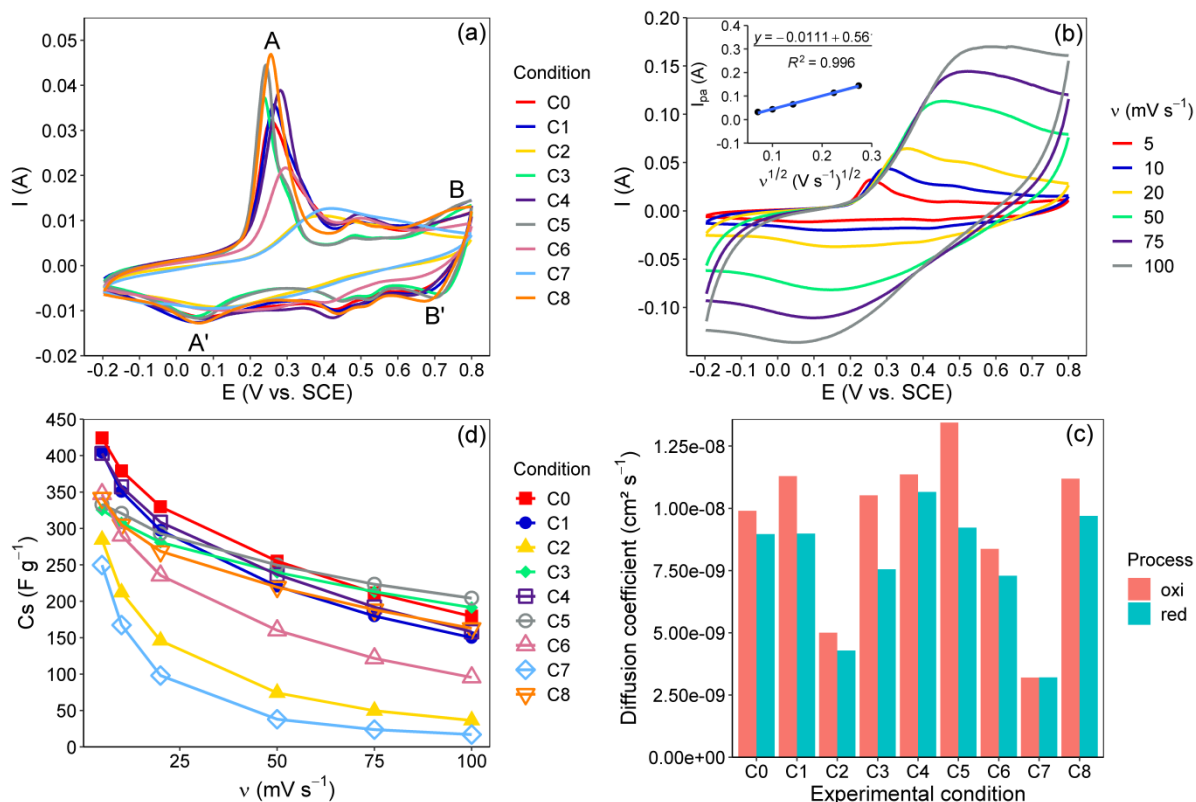


Fig. 4. (a) Cyclic voltammograms (CV) curves for samples obtained at different reaction conditions using 5 mV s^{-1} potential scan rate; (b) CV curves for sample deposited under C0 condition with varying potential scan rates (inset shown in the Graphic shows the linear plot relating I_{pa} vs. $v^{0.5}$); (c) dependence of specific capacitance (C_s) with the potential scan rate for samples obtained at different reaction conditions; (d) diffusion coefficients for samples obtained under different reaction conditions.

A linear relation was found between the anodic current peaks related to the transition between leucoemeraldine/emeraldine forms as a function of the square root of the potential scan rate, as shown in Figure 4b (inset). This behavior is typical of diffusion-controlled electrochemical processes, being observed for all samples in both cathodic and anodic processes. Thus, charge diffusion coefficients were estimated using the Randles-Sevcik equation (2) (Firda *et al.*, 2021):

$$I_p = -0,446nFAC \left(\frac{nFvD}{RT} \right)^{0,5} \quad (2)$$

where I_p is the anodic peak current (A); v is the potential scan rate (V s^{-1}); n is the number of electrons transferred in the redox reaction; F is the Faraday constant (C mol^{-1}); A is the surface area of the electrode (cm^2); C is the electrolyte concentration (mol cm^{-3}); D is the electrolyte's diffusion coefficient ($\text{cm}^2 \text{ s}^{-1}$); R is the gas constant ($8,314 \text{ J mol}^{-1} \text{ K}^{-1}$); and T is the temperature of the electrochemical cell (K). The charge diffusion coefficient related to anodic and cathodic peaks in CV curves are shown in Fig. 4c. In general, larger diffusion coefficients were observed during oxidation than during reduction, indicating that the kinetics of the process favors the oxidized state. Moreover, the diffusion coefficients exhibited values between 3.20×10^{-9} and $1.34 \times 10^{-8} \text{ cm}^2 \text{ s}^{-1}$, in agreement to values reported in the literature (Popov *et al.*, 2019; Wang *et al.*, 2013).

C. Data analysis of experimental design

The effect of oxidant/monomer ratio (rOM) and of acidity (Ac) on the specific capacitance of PANI film electrodes were evaluated through a central composite circumscribed design (see Tab. 2 for conditions). The values of specific capacitance used as response variable were determined from CV measurements (5 mV s^{-1} , Tab.4). Multiple linear regression analysis (MLR) of resulting data was applied to determination and yielded the following expression:

$$y = 428,78 - 3,40.rOM + 19,25.Ac + 48,41.rOM:Ac - 39,55.rOM^2 - 42,72.Ac^2$$

where rOM (oxidant/monomer ratio), Ac (acid molar concentration), rOM:Ac (interaction term), rOM² (quadratic rOM) and Ac² (quadratic A) are the independent variables. The determination coefficient (R²) obtained for this model was 0.9317, indicating that the model is able to explain 93.17% of data variability.

Tab. 4. Specific capacitance for PANI electrodes determined at 5 mV s⁻¹.

Condition	C1	C2	C3	C4	C0	C0	C0	C5	C6	C7	C8
C _s (F g ⁻¹)	404.5	284.4	325.6	403.1	424.9	420.5	427.2	332.8	347.2	249.7	341.9

The significance of the model's coefficients was analyzed through ANOVA (Tab. 3) and indicate that only the main rOM effect didn't influence significantly the specific capacitance, while other coefficients showed p values below 5% of significance. Thus, this analysis allowed to maintain the coded regression model including quadratic terms representing the curvature region corresponding to experimental data could.

Tab. 5. Analysis of variance (ANOVA) for data resulting from the central composite circumscribed design.

Source of variation	Degree of freedom	Sum of squares	Mean square	F	p-value
rOM	1	63	63	0.074	0.796
Ac	1	3622	3622	4.295	0.093
rOM ²	1	1744	1744	2.068	0.210
Ac ²	1	17128	17128	20.312	0.006
rOM:Ac	1	9769	9769	11.586	0.0192
Residues	5	4216	843	-	-

It was possible to represent graphically the experimental region evaluated in the form of a response surface considering the regression model (Fig. 5). The resulting plots allow a fast visualization and an easy understanding of the dependence of the response on the variables studied. Thus, the presence of quadratic terms in the model leads to a curved region with maximum specific capacitance value (426.8 F g⁻¹). The combination of the factors leading to the maximum point, known as optimum point, corresponding to this point are rOM = 1.15 and 1.64 molL⁻¹ H₂SO₄.

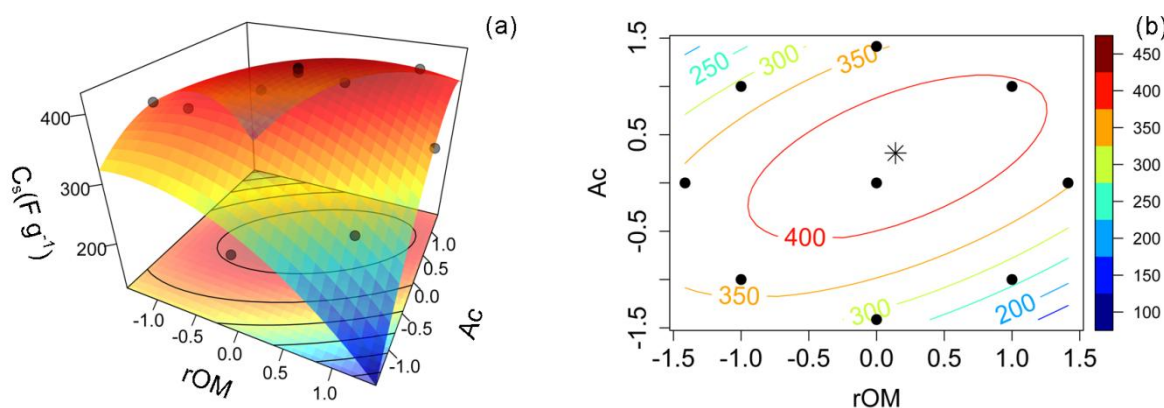


Fig. 5. (a) Surface response plot and (b) contour plot showing the behavior of specific capacitance for PANI film electrodes as function of the oxidant/monomer ratio and acidity of the reaction medium.

IV. CONCLUSION

PANI film electrodes were prepared successfully through microwave-assisted-CBD method. The experimental conditions with the highest acidity (C3 and C8) in addition to lowest oxidant/monomer ratio positively affected the polymerization kinetics of PANI and consequently lead to the highest deposition rates. PANI formation in its conductive form emeraldine salt was evidenced through vibration bands present in FTIR spectra. Moreover, an estimation of the oxidation degree of PANI was also possible from the relative intensity of bands assigned to quinoid to those assigned to benzenoid rings (I_Q/I_B). Those ratios indicated that the oxidation degree tends to increase as the concentrations of both acid and oxidant increase in the reaction

medium. Cyclic voltammetry curves pointed out that the PANI film electrodes exhibited pseudocapacitive behavior, with diffusion controlled kinetics of redox reactions. Finally, a central composite circumscribed design was used to investigate the effect of the oxidant/monomer ration and the acid dopant concentration on the specific capacitance of films. This study revealed that the factors evaluated had significant effects on the specific capacitance. Also, the surface response plot presented a combination of variables leading to optimal capacitance (426.8 F g^{-1}), occurring at O/M = 1.15 and concentration of H_2SO_4 of 1.64 mol L^{-1} .

REFERENCES

- [1]. ABDIRYIM, T.; XIAO-GANG, Z.; JAMAL, R. Comparative studies of solid-state synthesized polyaniline doped with inorganic acids. *Materials Chemistry and Physics*, v. 90, n. 2–3, p. 367–372, 2005.
- [2]. ARULMANI, S.; WU, J. J.; ANANDAN, S. Ultrasound promoted transition metal doped polyaniline nanofibers: Enhanced electrode material for electrochemical energy storage applications. *Ultrasonics Sonochemistry*, v. 51, n. July 2018, p. 469–477, 2019.
- [3]. DENG, J.; WANG, X.; GUO, J.; LIU, P. Effect of the oxidant/monomer ratio and the washing post-treatment on electrochemical properties of conductive polymers. *Industrial and Engineering Chemistry Research*, v. 53, n. 35, p. 13680–13689, 2014.
- [4]. DESHMUKH, P. R.; BULAKHE, R. N.; PUSAWALE, S. N.; SARTALE, S. D.; LOKHANDE, C. D. Polyaniline– RuO_2 composite for high performance supercapacitors: chemical synthesis and properties. *RSC Advances*, v. 5, n. 36, p. 28687–28695, 2015.
- [5]. DESHMUKH, P. R.; PUSAWALE, S. N.; JAMADADE, V. S.; PATIL, U. M.; LOKHANDE, C. D. Microwave assisted chemical bath deposited polyaniline films for supercapacitor application. *Journal of Alloys and Compounds*, v. 509, n. 16, p. 5064–5069, 2011.
- [6]. DESHMUKH, P. R.; SHINDE, N. M.; PATIL, S. V.; BULAKHE, R. N.; LOKHANDE, C. D. Supercapacitive behavior of polyaniline thin films deposited on fluorine doped tin oxide (FTO) substrates by microwave-assisted chemical route. *Chemical Engineering Journal*, v. 223, p. 572–577, 2013.
- [7]. DINARI, M.; MOMENI, M. M.; GOUDARZIRAD, M. Nanocomposite films of polyaniline/graphene quantum dots and its supercapacitor properties. *Surface Engineering*, v. 32, n. 7, p. 535–540, 2016.
- [8]. FIRDA, P. B. D.; MALIK, Y. T.; OH, J. K.; WUJCIK, E. K.; JEON, J. W. Enhanced chemical and electrochemical stability of polyaniline-based layer-by-layer films. *Polymers*, v. 13, n. 17, p. 1–13, 2021.
- [9]. FOROUZANDEH, P.; KUMARAVEL, V.; PILLAI, S. C. Electrode materials for supercapacitors: A review of recent advances. *Catalysts*, v. 10, n. 9, p. 1–73, 2020.
- [10]. GOLBA, S.; POPCZYK, M.; MIGA, S.; JUREK-SULIGA, J.; ZUBKO, M.; KUBISZTAL, J.; BALIN, K. Impact of acidity profile on nascent polyaniline in the modified rapid mixing process—material electrical conductivity and morphological study. *Materials*, v. 13, n. 22, p. 1–15, 2020.
- [11]. HAN, Y.; DAI, L. Conducting Polymers for Flexible Supercapacitors. *Macromolecular Chemistry and Physics*, v. 220, n. 3, p. 1–14, 2019.
- [12]. HE, X.; ZHANG, X. A comprehensive review of supercapacitors: Properties, electrodes, electrolytes and thermal management systems based on phase change materials. *Journal of Energy Storage*, v. 56, n. PC, p. 106023, 2022.
- [13]. MAZZEU, M. A. C.; FARIA, L. K.; BALDAN, M. R.; REZENDE, M. C.; GONÇALVES, E. S. Influence of reaction time on the structure of polyaniline synthesized on a pre-pilot scale. *Brazilian Journal of Chemical Engineering*, v. 35, n. 1, p. 123–130, 2018.
- [14]. MELLO, H. J. N. P. D.; MULATO, M. Effect of aniline monomer concentration on PANI electropolymerization process and its influence for applications in chemical sensors. *Synthetic Metals*, v. 239, n. March, p. 66–70, 2018.
- [15]. MISNON, I. I.; JOSE, R. Synthesis and electrochemical evaluation of the PANI/ δ - MnO_2 electrode for high performing asymmetric supercapacitors. *New Journal of Chemistry*, v. 41, n. 14, p. 6574–6584, 2017.
- [16]. PENG, X. Y.; LUAN, F.; LIU, X. X.; DIAMOND, D.; LAU, K. T. pH-controlled morphological structure of polyaniline during electrochemical deposition. *Electrochimica Acta*, v. 54, n. 26, p. 6172–6177, 2009.
- [17]. POPOV, A.; BRASIUNAS, B.; MIKOLIUNAITE, L.; BAGDZIUNAS, G.; RAMANAVICIUS, A.; RAMANAVICIENE, A. Comparative study of polyaniline (PANI), poly(3,4-ethylenedioxythiophene) (PEDOT) and PANI-PEDOT films electrochemically deposited on transparent indium thin oxide based electrodes. *Polymer*, v. 172, n. January, p. 133–141, 2019.
- [18]. QIU, B.; LI, Z.; WANG, X.; LI, X.; ZHANG, J. Exploration on the microwave-assisted synthesis and formation mechanism of polyaniline nanostructures synthesized in different hydrochloric acid concentrations. *Journal of Polymer Science, Part A: Polymer Chemistry*, v. 55, n. 20, p. 3357–3369, 2017.
- [19]. QIU, B.; WANG, J.; LI, Z.; WANG, X.; LI, X. Influence of acidity and oxidant concentration on the nanostructures and electrochemical performance of polyaniline during fast microwave-assisted chemical polymerization. *Polymers*, v. 12, n. 2, 2020.
- [20]. SANTINO, L. M.; LU, Y.; ACHARYA, S.; BLOOM, L.; COTTON, D.; WAYNE, A.; D'ARCY, J. M. Enhancing Cycling Stability of Aqueous Polyaniline Electrochemical Capacitors. *ACS Applied Materials and Interfaces*, v. 8, n. 43, p. 29452–29460, 2016.
- [21]. SAPURINA, I.; STEJSKAL, J. The mechanism of the oxidative polymerization of aniline and the formation of supramolecular polyaniline structures. *Polymer International*, v. 57, n. 12, p. 1295–1325, dez. 2008.
- [22]. SAPURINA, I. Y.; SHISHOV, M. A. Oxidative Polymerization of Aniline: Molecular Synthesis of Polyaniline and the Formation of Supramolecular Structures. In: INTECHOPEN (Ed.). *New Polymers for Special Applications*. [s.l.] InTech, 2012. p. 251–312.
- [23]. SARDANA, S.; GUPTA, A.; SINGH, K.; MAAN, A. S.; OHLAN, A. Conducting polymer hydrogel based electrode materials for supercapacitor applications. *Journal of Energy Storage*, v. 45, n. September 2021, p. 103510, 2022.
- [24]. SENGUPTA, S.; AGGARWAL, R.; RAULA, M. A review on chemical bath deposition of metal chalcogenide thin films for heterojunction solar cells. *Journal of Materials Research*, p. 1–12, 2022.
- [25]. TRCHOVÁ, M.; STEJSKAL, J. Polyaniline: The infrared spectroscopy of conducting polymer nanotubes (IUPAC Technical Report). *Pure and Applied Chemistry*, v. 83, n. 10, p. 1803–1817, 2011.
- [26]. TURAN, E.; ZEYBEKOĞLU, E.; KUL, M. Effects of bath temperature and deposition time on Co_3O_4 thin films produced by chemical bath deposition. *Thin Solid Films*, v. 692, n. June 2018, 2019.
- [27]. VENKATESH, S.; VISHISTA, K. Identification of the best chemical equivalent ratio to produce emeraldine salt exhibiting better pseudo capacitance. *Electrochimica Acta*, v. 263, p. 76–84, 2018.
- [28]. WANG, J.; NING, Y.; WEN, YUFENG; WEN, YANG; DONG, T.; WANG, D.; CHEN, J.; ZHANG, L. Characteristics and

- electrochemical reaction kinetics of polyaniline nanofibers as a promoter of pt electrode for methanol electrocatalytic oxidation. **Zeitschrift fur Physikalische Chemie**, v. 227, n. 1, p. 89–103, 2013.
- [29]. YAVUZ, A.; YILMAZ ERDOGAN, P.; ZENGIN, H. The use of polyaniline films on flexible tape for supercapacitor applications. **International Journal of Energy Research**, v. 44, n. 14, p. 11941–11955, 2020.